Magnetic Fullerenes inside Single-Wall Carbon Nanotubes

F. Simon,[1,3,*] H. Kuzmany,[1] B. Náfrádi,[2] T. Fehér,[2,3] L. Forró,[2] F. Fülöp,[3] A. Jánossy,[3] L. Korecz,[4] A. Rockenbauer,[4] F. Hauke,[5] and A. Hirsch[5]

[1]*Institut für Materialphysik, Universität Wien, Strudlhofgasse 4, A-1090 Wien, Austria*
[2]*Institute of Physics of Complex Matter, FBS Swiss Federal Institute of Technology (EPFL), CH-1015 Lausanne, Switzerland*
[3]*Institute of Physics and Solids in Magnetic Fields Research Group of the Hungarian Academy of Sciences, Budapest University of Technology and Economics, P.O. Box 91, H-1521 Budapest, Hungary*
[4]*Chemical Research Center, Institute of Chemistry, P.O. Box 17, H-1525 Budapest, Hungary*
[5]*Institut für Organische Chemie der Friedrich Alexander Universität Erlangen-Nürnberg, Henkestrasse 42, D-91054 Erlangen, Germany*

(Received 18 June 2006; published 25 September 2006)

$C_{59}N$ magnetic fullerenes were formed inside single-wall carbon nanotubes by vacuum annealing functionalized $C_{59}N$ molecules encapsulated inside the tubes. A hindered, anisotropic rotation of $C_{59}N$ was deduced from the temperature dependence of the electron spin resonance spectra near room temperature. Shortening of the spin-lattice relaxation time T_1 of $C_{59}N$ indicates a reversible charge transfer toward the host nanotubes above ~350 K. Bound $C_{59}N$-C_{60} heterodimers are formed at lower temperatures when C_{60} is coencapsulated with the functionalized $C_{59}N$. In the 10–300 K range, T_1 of the heterodimer shows a relaxation dominated by the conduction electrons on the nanotubes.

DOI: 10.1103/PhysRevLett.97.136801 PACS numbers: 73.63.Fg, 72.80.Rj, 76.30.−v

Single-wall carbon nanotubes (SWCNTs) [1,2] exhibit unusual physical phenomena related to their one-dimensional and strongly correlated electronic properties. These include excitonic effects [3,4], superconductivity [5], the Tomonaga-Luttinger liquid state [6], and the Peierls transition [7]. Magnetic resonance is a powerful method to study strong correlations in low-dimensional systems. However, for SWCNTs, both nuclear magnetic resonance (NMR) and electron spin resonance (ESR) are limited by NMR active ^{13}C nuclei and ESR active electron spins in residual magnetic catalytic particles and other carbon phases. Synthesis of ^{13}C isotope engineered SWCNTs solved the problem for NMR [8,9]. To enable ESR spectroscopy of SWCNTs, a local probe, specifically attached to SWCNTs, is required. The $N@C_{60}$ [10] and $C_{59}N$ [11] magnetic fullerenes are ideal candidates for such studies. In fullerene doped SWCNTs, fullerenes occupy preferentially the interior of the tubes and form ''peapods'' (C_{60}@SWCNT) [12]. Fullerenes adhering to the outside can be removed [13] in contrast to, e.g., filling with iron [14]. ESR on encapsulated magnetic fullerenes could yield information on the electronic state of the tubes and on the fullerene rotational dynamics in a confined environment. In addition, magnetic fullerene peapods could enable a bottom-up design for magnetic storage devices or for building elements of quantum computers [15].

Typical spin concentrations in ($N@C_{60}$:C_{60}@SWCNT) are low, ~1 spin/tube, and the N spins are insensitive to SWCNT properties [16]. The $C_{59}N$ monomer radical is a better local probe candidate as the unpaired electron is on the cage. $C_{59}N$ can be chemically prepared, but it forms spinless dimers $(C_{59}N)_2$ or monomer adducts [11]. The magnetic $C_{59}N$ monomer radical can be stabilized as $C_{59}N$:C_{60}, a dilute solid solution of $C_{59}N$ in C_{60} [17].

Here we report on the first ESR study of SWCNT properties and peapod rotational dynamics using a paramagnetic local probe: $C_{59}N$ monomer radicals encapsulated inside SWCNTs. SWCNTs were first filled with chemically inert $C_{59}N$ derivatives. A heat treatment in vacuum removes the sidegroup, and the monomer radical is left behind. The rotation of encapsulated $C_{59}N$ is hindered and anisotropic in contrast to the isotropic rotation in $C_{59}N$:C_{60}. In samples with coencapsulated C_{60} and $C_{59}N$, bound $C_{59}N$-C_{60} heterodimers are formed during the heat treatment. The electron spin-relaxation time of the heterodimer is dominated by the conduction electrons of the SWCNTs and follows the Korringa law.

SWCNTs were filled with air stable $C_{59}N$ derivatives (4-hydroxy-3,5-dimethyl-phenyl-hydroazafullerene, $C_{59}N$-der in the following) and $C_{59}N$-der:C_{60} in concentrations of 1:10. The mean value of the SWCNT diameter distribution, as determined from Raman studies [18], $d = 1.40$ nm is optimal for fullerene encapsulation. A mixture of dissolved fullerenes and SWCNTs was sonicated in toluene and filtered. This results in a high degree of encapsulation and ensures that fullerenes remain only inside the tubes as shown by transmission electron microscopy and Raman spectroscopy in Ref. [19]. The peapods were mixed with ESR silent SnO_2 to separate the conducting SWCNT pieces and were annealed in dynamic vacuum at 600 °C for 15 min to remove the sidegroup. The air-sensitive materials were sealed under He in quartz tubes. ESR was studied on a Bruker spectrometer at 9 GHz in the 10–600 K temperature range with sensitivity calibrated by $CuSO_4 \cdot 5(H_2O)$.

Figure 1 shows the room temperature ESR spectra of $C_{59}N$@SWCNT (sample a) and $C_{59}N$:C_{60}@SWCNT (sample b) and, for comparison, the spectrum of crystalline $C_{59}N$:C_{60} (sample c) from Ref. [17]. This latter spectrum

was previously assigned to the superposition of rotating $C_{59}N$ monomers and bound $C_{59}N$-C_{60} heterodimers [20]. The large spin density at the ^{14}N nucleus of the rotating $C_{59}N$ molecule results in an ESR triplet signal, and the $C_{59}N$-C_{60} heterodimer has a singlet signal [arrow in Fig. 1(c)] as the spin density resides on the C_{60} molecule. ^{14}N triplet structures are observed in the peapod samples (a and b) with hyperfine coupling $A = 0.368(3)$ mT and g factor $g = 2.0013(2)$, identical to the crystalline sample (c) and are, thus, identified as rotating $C_{59}N$ monomer radicals encapsulated inside SWCNTs. The additional component [arrow in Fig. 1(b)] observed for sample b, which contains coencapsulated C_{60}, is identified as $C_{59}N$- C_{60} heterodimers encapsulated inside SWCNTs since this signal has the same g factor $g = 2.0024(2)$ as the crystalline material. This singlet line is absent in sample a, which does not contain C_{60}. For both peapod samples, a broader line with a HWHM of $\Delta H \sim 0.6$ mT is also observed. The broader component appears also on heat treatment of reference samples without encapsulated $C_{59}N$-der and is identified as a side product. Annealing at 600 °C is optimal: Lower temperatures result in smaller $C_{59}N$ signals, and higher temperatures increase the broad impurity signal without increasing the $C_{59}N$ intensity.

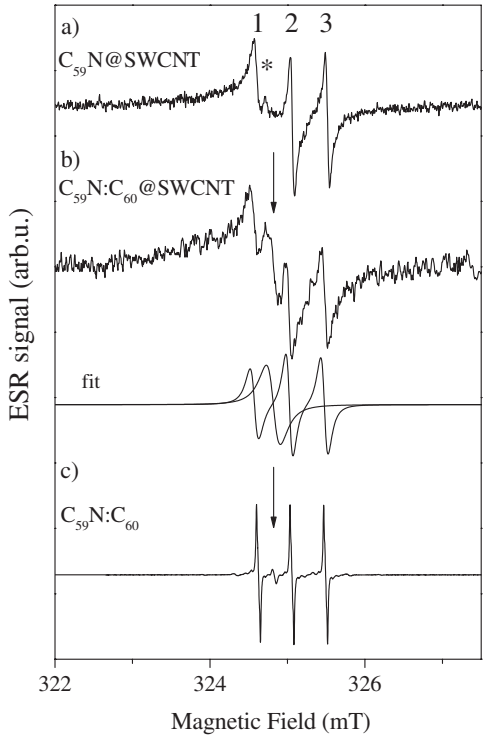

FIG. 1. ESR spectra of (a) $C_{59}N$@SWCNT, (b) $C_{59}N$:C_{60}@SWCNT, and (c) crystalline $C_{59}N$:C_{60} at 300 K. 1, 2, and 3 denote the ^{14}N hyperfine triplet lines with a nuclear state of $I = 1$, 0, and -1, respectively. The asterisk in (a) shows a weak impurity signal. The arrows in (b) and (c) indicate the $C_{59}N$-C_{60} heterodimer. The fit in (b) shows the deconvolution of the ESR signal into the ^{14}N triplet of monomer $C_{59}N$ and the $C_{59}N$-C_{60} heterodimer components.

Deconvolution of the ESR signal [Fig. 1(b)] and the intensity calibration allows one to measure the amount of $C_{59}N$ related ($C_{59}N$ monomer and $C_{59}N$- C_{60} heterodimer) spins in the sample. The amount of encapsulated fullerenes is known [8]; thus, the ratio r of observed $C_{59}N$ related spins and encapsulated $C_{59}N$-der can be determined. We obtained $r = 2.5(6)\%$ and $r = 12(3)\%$ for the a and b samples, respectively. The observed ESR signal of $C_{59}N$ can be reduced due to various reasons: (i) dimerization of $C_{59}N$ first neighbors into ESR silent $(C_{59}N)_2$, (ii) incomplete transformation of $C_{59}N$-der into $C_{59}N$, (iii) dipolar fields of near neighbor $C_{59}N$ pairs: Only those $C_{59}N$ related spins are observed which have no neighbors with dipole fields larger than the ESR linewidth ~0.07 mT. The likely origin of the smaller r value for sample a is dimerization. For sample b, however, a statistical calculation of the dipolar fields gives $r = 9\%$, in agreement with the experimental value. For the calculation, the fullerene lattice constant inside the tubes [21], the three-dimensional arrangement of the SWCNTs into bundles [22], the random orientation of the bundles, and the concentration of $C_{59}N$ was taken into account. As a result, the data for sample b support that most $C_{59}N$-der is transformed to $C_{59}N$ monomer radicals.

The temperature dependence of the linewidths of the ^{14}N triplet is identical for the two peapod samples, a and b, and is shown together with the data on $C_{59}N$:C_{60} in Fig. 2 using the labeling given in Fig. 1(a). The linewidths are ~0.04 mT larger for the peapod than for the crystalline material. This excess linewidth is similar to that of (N@C_{60}:C_{60})@SWCNT and is related to the stray magnetic field of magnetic catalytic particles in the nanotube sample [16]. The three $C_{59}N$ triplet lines are broadened unequally at lower temperatures for both the peapod and crystalline materials. The details of the low temperature broadening are different for the two kinds of materials: For encapsulated $C_{59}N$, the inequality persists to higher temperatures, and the three lines broaden differently, whereas for the crystalline $C_{59}N$:C_{60}, line 1 broadens significantly and lines 2 and 3 broaden equally but less.

The unequal broadening of ^{14}N triplet lines with decreasing temperature is well known for NO spin labels and is explained by an incomplete motional narrowing of the anisotropic hyperfine and g-factor anisotropy [23]. For crystalline $C_{59}N$:C_{60}, molecular rotation becomes rapid enough above the 261 K structural transition to result in motionally narrowed lines [17]. In contrast, the linewidth of encapsulated $C_{59}N$ indicates a hindered rotation. The linewidth for hindered molecular rotation is

$$\Delta H = A + BM_I + CM_I^2, \quad (1)$$

where M_I is the nuclear state of the ^{14}N hyperfine lines and the parameters A, B, and C depend on the hyperfine and g-tensor components, on the R_x, R_y, and R_z molecular rotational rates around each axis, and on the ESR frequency [23]. For crystalline $C_{59}N$:C_{60} at 9 GHz, the iso-

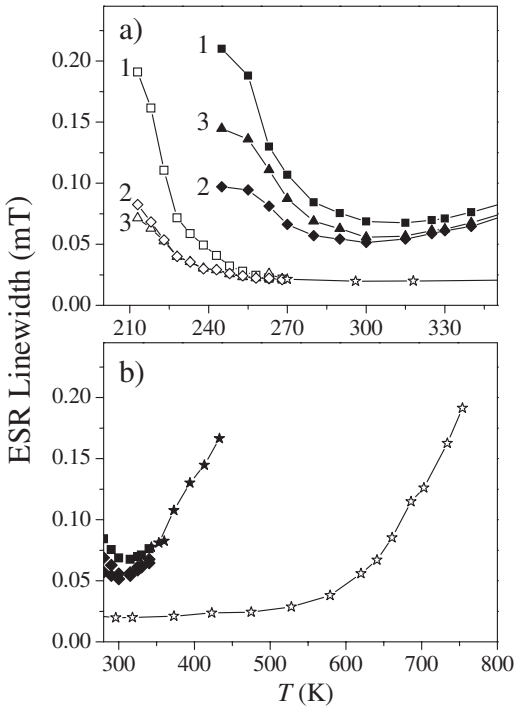

FIG. 2. Linewidths of the ^{14}N triplet components in crystalline $C_{59}N$:C_{60} (open symbols) and ($C_{59}N$, $C_{59}N$:C_{60})@SWCNT (solid symbols) samples (a) below 350 K and (b) above 290 K. The stars show the data for the temperature range where the linewidths of the three components are equal. The solid lines are guides to the eye.

tropic rotation of the molecule (i.e., $R_x = R_y = R_z$) combined with the hyperfine and g tensors results in $B \approx C$ and, thus, in an equal broadening for lines 2 ($M_I = 0$) and 3 ($M_I = -1$) [17,20]. The inequality of the linewidths for encapsulated $C_{59}N$ indicates an anisotropic rotation, i.e., $R_x \neq R_y \neq R_z$, which is suggested to originate from the anisotropic environment inside the nanotubes.

Above 300 K, the triplet linewidths rapidly grow with temperature [Fig. 2(b)] and the signal intensity decreases faster than the Curie law but no new lines appear. The broadening and the loss of signal intensity is reversible with temperature cycling. The broadening is reminiscent of that observed above ~600 K in the crystalline material, which was interpreted as a spin-lattice lifetime shortening due to delocalization of the electron from $C_{59}N$ over the C_{60} matrix [20]. Based on the analogous behavior, we suggest that reversible charge transfer from $C_{59}N$ to the nanotubes takes place above ~350 K. The lower temperature of the charge transfer indicates a larger overlap of the extra electron of $C_{59}N$ to the SWCNTs compared to its overlap with the C_{60} conduction band in the crystalline material. In $C_{59}N$:C_{60}, the broadening is accompanied by the emergence of the ESR signal of the delocalized electrons. The intrinsic ESR signal of SWCNTs is not observable [24,25], which explains the absence of the signal of charge transferred electrons on the tubes.

The coexistence of bound $C_{59}N$-C_{60} heterodimers and rotating $C_{59}N$ molecules was understood for $C_{59}N$:C_{60} as a thermal equilibrium between the ground state heterodimer and the rotating monomers [20]. The inset in Fig. 3 shows a similar behavior for $C_{59}N$:C_{60}@SWCNT: The heterodimer dominates the low temperature spectrum and vanishes at higher temperatures; however, the relative intensity of the heterodimer is much larger. The heterodimer signal intensity normalized by the total (heterodimer + triplet) intensity gives the heterodimer concentration and is shown in Fig. 3. Similarly to crystalline $C_{59}N$:C_{60}, the heterodimer concentration can be fitted with:

$$\frac{I_{C_{59}N\text{-}C_{60}}}{I_{\text{total}}} = \frac{1}{(1 + e^{(-E_a/T+\Delta S)})}, \qquad (2)$$

where E_a is the binding energy of the heterodimer, and ΔS is the entropy difference between the rotating monomer and the static heterodimer states. A fit with Eq. (2) for the peapod material is shown in Fig. 3 as a solid curve and gives E_a(peapod) = 2800(200) K and ΔS(peapod) = 9(1). This compares to the results for the crystalline material with E_a(cryst) = 2400(600) K and ΔS(cryst) = 11(2) [20]. The higher heterodimer concentrations for the peapod material are caused by the larger E_a and/or smaller ΔS values. The latter is explained by the limited rotational freedom of encapsulated $C_{59}N$.

Similar to NMR, the ESR spin-lattice relaxation time T_1 of the heterodimer spins yields information on the electronic structure of the host SWCNTs [26]. T_1 can be measured by time-resolved ESR or in continuous wave ESR from the linewidth ΔH by separating the homogeneous, relaxation related linewidth from the inhomogeneous one. In Fig. 4(a), we show ΔH for the heterodimer signal as determined from fits with derivative Lorentzian lines. Clearly, ΔH has a temperature dependent component in addition to a $\Delta H_0 = 0.089(2)$ mT residual linewidth,

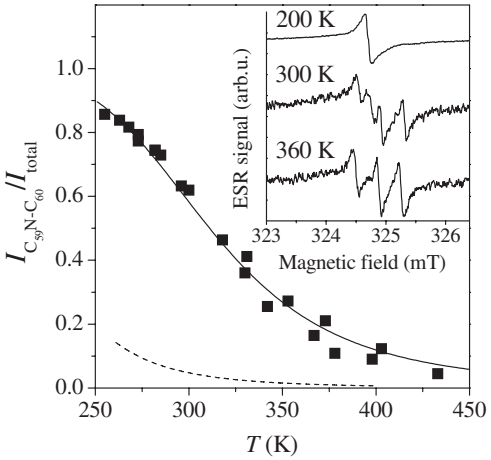

FIG. 3. Concentration of $C_{59}N$-C_{60} bound heterodimers in $C_{59}N$:C_{60}@SWCNT. The solid curve is a fit with parameters explained in the text. The dashed curve shows the same quantity for crystalline $C_{59}N$:C_{60} above the 261 K phase transition. Note the much higher heterodimer concentration for the peapod material. The inset shows the temperature evolution of the spectra.

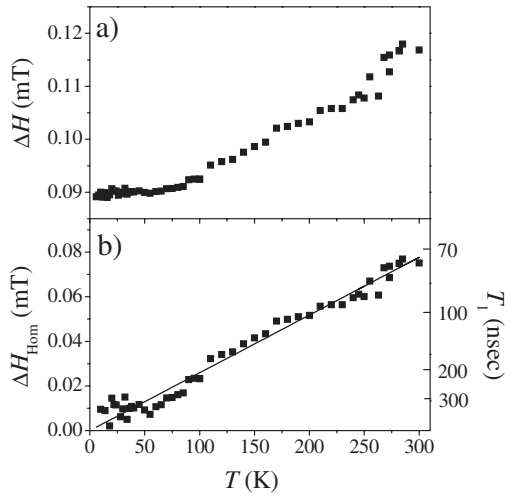

FIG. 4. (a) Temperature dependence of the ESR linewidth for the heterodimer signal. (b) The homogeneous contribution to the linewidth with a linear fit (solid line). The corresponding T_1 values are shown on the right axis.

which is obtained by averaging the linewidths below 50 K. The line shape of the heterodimer signal does not change with temperature, which indicates a uniform, homogeneous broadening in addition to the inhomogeneous residual width. NMR studies on nanotube samples [9] prepared from the same source of SWCNTs prove that magnetic particles or other defects do not affect the temperature dependent linewidth.

To obtain the homogeneous linewidth ΔH_{Hom}, we subtracted ΔH_0 from the linewidth data: $\Delta H_{\mathrm{Hom}} = \sqrt{\Delta H^2 - \Delta H_0^2}$. Figure 4(b) shows ΔH_{Hom} and $1/T_1 = \gamma_e \Delta H_{\mathrm{Hom}}$, where $\gamma_e/2\pi = 28.0$ GHz/T is the electron gyromagnetic ratio. $1/T_1$ as a function of T is linear, with $(T_1 T)^{-1} = 4.2(2) \cdot 10^4\ (\mathrm{s\,K})^{-1}$ [fit shown in Fig. 4(b)], which suggests that Korringa relaxation, i.e., the interaction with conduction electrons [26], gives the relaxation of the heterodimer. An effective coupling constant (averaged for tube chiralities) A of localized spins and conduction electrons is 11 meV as determined from the Korringa relation [26]:

$$\frac{1}{T_1 T} = \left(\frac{4\pi k_B}{\hbar}\right) A^2 \bar{n}(E_F)^2, \tag{3}$$

where $\bar{n}(E_F) = 0.014$ (states/eV)/atom is the density of states (DOS) at the Fermi level for a $d \approx 1.4$ nm metallic tube in the tight-binding approximation [22]. The uniform homogeneous broadening suggests that the heterodimer spins do not sense separate metallic and semiconducting tubes as would be expected from the tube geometry [22]. This can be explained by charge transfer in the SWCNTs bundles, which shifts the Fermi level and renders all tubes metallic.

In summary, we observed $C_{59}N$ monomer radicals inside SWCNTs. The nanotube cage hinders and makes the molecular rotation anisotropic. We find a low activation energy for charge transfer to the tubes. At low temperatures, bound $C_{59}N$-C_{60} heterodimers are observed when mixtures of the two fullerenes are encapsulated. Electron spin relaxation of the heterodimer shows an overall metallic behavior of the tubes. The material is a step toward the realization of confined linear spin chains, which might find application in, e.g., quantum information processing.

F. S. acknowledges the Zoltán Magyary program for support. This work was supported by the Austrian Science Funds (FWF) Project No. 17345, by the Deutsche Forschungsgemeinschaft (DFG), by the EU Projects No. MERG-CT-2005-022103 and No. HPRN-CT-2002-00192, and by the Hungarian State Grants (OTKA) No. TS049881, No. F61733, No. PF63954, No. NK60984, and No. T046953.

*Corresponding author.
Electronic address: ferenc.simon@univie.ac.at

[1] S. Iijima and T. Ichihashi, Nature (London) **363**, 603 (1993).
[2] D. S. Bethune *et al.*, Nature (London) **363**, 605 (1993).
[3] C. D. Spataru *et al.*, Phys. Rev. Lett. **92**, 077402 (2004).
[4] F. Wang, G. Dukovic, L. E. Brus, and T. F. Heinz, Science **308**, 838 (2005).
[5] Z. K. Tang *et al.*, Science **292**, 2462 (2001).
[6] H. Ishii *et al.*, Nature (London) **426**, 540 (2003).
[7] K. P. Bohnen *et al.*, Phys. Rev. Lett. **93**, 245501 (2004).
[8] F. Simon *et al.*, Phys. Rev. Lett. **95**, 017401 (2005).
[9] P. M. Singer *et al.*, Phys. Rev. Lett. **95**, 236403 (2005).
[10] T. Almeida Murphy *et al.*, Phys. Rev. Lett. **77**, 1075 (1996).
[11] J. C. Hummelen, C. Bellavia-Lund, and F. Wudl, *Heterofullerenes* (Springer, Berlin, Heidelberg, 1999), Vol. 199, p. 93.
[12] B. W. Smith, M. Monthioux, and D. E. Luzzi, Nature (London) **396**, 323 (1998).
[13] H. Kataura *et al.*, Synth. Met. **121**, 1195 (2001).
[14] B. C. Satishkumar, A. Taubert, and D. E. Luzzi, J. Nanosci. Nanotech. **3**, 159 (2003).
[15] W. Harneit *et al.*, Phys. Status Solidi B **233**, 453 (2002).
[16] F. Simon *et al.*, Chem. Phys. Lett. **383**, 362 (2004).
[17] F. Fülöp *et al.*, Chem. Phys. Lett. **334**, 233 (2001).
[18] H. Kuzmany *et al.*, Eur. Phys. J. B **22**, 307 (2001).
[19] F. Simon *et al.*, Carbon **44**, 1958 (2006).
[20] A. Rockenbauer *et al.*, Phys. Rev. Lett. **94**, 066603 (2005).
[21] K. Hirahara *et al.*, Phys. Rev. B **64**, 115420 (2001).
[22] M. S. Dresselhaus, G. Dresselhaus, and P. Avouris, *Carbon Nanotubes: Synthesis, Structure, Properties, and Applications* (Springer, Berlin, 2001).
[23] J. H. Freed, *Spin Labeling: Theory and Application*, edited by L. J. Berliner (Academic, New York, 1976), pp. 53–132.
[24] A. S. Claye, N. M. Nemes, A. Jánossy, and J. E. Fischer, Phys. Rev. B **62**, R4845 (2000).
[25] J.-P. Salvetat *et al.*, Phys. Rev. B **72**, 075440 (2005).
[26] C. P. Slichter, *Principles of Magnetic Resonance* (Springer-Verlag, New York, 1989), 3rd ed.